Computers and Electronics in Agriculture 198 (2022) 106981

Contents lists available at ScienceDirect

Computers and Electronics in Agriculture

journal homepage: www.elsevier.com/locate/compag

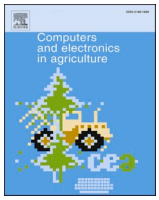

Acoustics applied in the development of equipment for precision agriculture: Coffee handling and harvesting

Geovanne P. Furriel [a,b,*], Brunna C.R.S. Furriel [a,c], Antônio P. Coimbra [d], Wesley P. Calixto [a,c,*]

[a] Electrical, Mechanical and Computer Engineering School/Federal University of Goias, Goiania, Goias, Brazil
[b] Agroindustrial Automation and Energy Efficiency Group/Federal Institute Goiano, Trindade, Goias, Brazil
[c] Studies and Researches in Science and Technology Group/Federal Institute of Goias, Goiania, Goias Brazil
[d] Institute of Systems and Robotics/University of Coimbra, Portugal

ARTICLE INFO

Keywords:
Agriculture
Acoustic
Similitude
Simulation
Coffee

ABSTRACT

This work presents a methodology for developing two types of equipment for precision agriculture applied in coffee handling and harvesting, based on acoustic techniques. The proposed methodology uses the similitude method to simulate induced vibration and the direction of sound pressure fields. After analyzing the scale reduction model, a prototype is built in real dimensions to validate the proposed system. Two acoustic induction systems are evaluated: (i) application of phytosanitary products and (ii) selective harvesting of fruits. In applying a phytosanitary product, there is a drift reduction and increase in leaf coverage by approximately 44.97%. In selective harvesting, the proposed method is analyzed, and approximately 40% of the fruits in the appropriate ripening stage were harvested. The presented acoustic techniques applied to agriculture are promising for developing equipment in precision coffee handling and harvesting. The results obtained indicate that using acoustic techniques in the harvest promotes the reduction of the inherent wear of the harvest in the plants.

1. Introduction

Acoustical studies address several areas of knowledge. It is presented as a principle of location, communication, or defense in the biological sciences. In human science is presented as speech, creating philosophy, and linguistics. For exacts science, acoustics has been examined in several aspects, manipulated as demand, such as amplifying its intensity, canceling noises, directing or distributing sounds, and translating musical notes, among several others.

Beranek et al. (2012) claim that sound is the acoustical science object of study, dealing with production, propagation from source to receiver, detection, and perception. Sound is described as a disorder propagated through an elastic medium that causes pressure changes or particles displacement detected by people or instruments. Among the acoustical divisions are acoustic architecture, psychoacoustic, electroacoustic, noise control, shock and vibration (Dunn et al., 2015).

The application of acoustics in agricultural sciences enables the development of several techniques such as noise cancellation for the comfort of agricultural machinery operators, generation of sounds for biological control, pest detection, soil moisture monitoring, vibrations for harvesting fruits, amongst several other applications (Desmet et al., 2003; Escola et al., 2020; Gorthi et al., 2020; Ebrahimi et al., 2013). Besides, countless innovations are taking place in precision agriculture due to the most diverse new technologies (Tang et al., 2021).

Studies of fruit vibration performed until 1969 are empirical with a high investment of time and equipment (Parchomchuk et al., 1971). In 1969, Crooke, Rand, and Parchomuchuk developed the theory that relates linear and nonlinear dynamics of the fruit-peduncle system to the detachment rate of the fruits (Cooke et al., 1969; Rand et al., 1970; Parchomchuk et al., 1971; Parchomchuk and Cooke, 1972). Following then, the number of studies on this topic has increased exponentially. The vibration analysis is applied to improve machine parameters and methods developed for agriculture, mainly focusing on selective fruit removal.

Tsatsarelis (1987) performs olive trees tests based on a model of two degrees of freedom of the fruit-peduncle system with external damping due to air resistance. The analysis of the vibration intensity indicates the ideal frequency and displacement for harvesting. The results obtained reinforce the possibility of fruit detachment with or without the peduncle according to the frequency used and a low influence of external damping.

Kimmel et al. (1992), motivated by the fact that the characteristic

* Corresponding authors.
E-mail addresses: geovanne.furriel@ifgoiano.edu.br (G.P. Furriel), wpcalixto@pq.cnpq.br (W.P. Calixto).

https://doi.org/10.1016/j.compag.2022.106981
Received 24 February 2021; Received in revised form 11 April 2022; Accepted 12 April 2022
Available online 6 May 2022

frequency of fruits and vegetables is strongly correlated to ripeness, developed experimental procedures to check the vibration modes in spherical fruits. A model of multiple degrees of freedom is developed based on the characteristic frequency obtained experimentally from the results.

Silva et al. (2012) analyze the detachment strength of coffee fruits as a metric for harvester regulation of vibration and operational speed. The results obtained show a difference between the states of green and cherry. It also indicates that the Novo Mundo variety is the one that has the lowest average force necessary for the detachment of the ripe fruit among those grown in Brazil.

Savary et al. (2011) present a study on the distribution of harvest forces using vibration induced in the canopy of orange trees and evaluate the detachment force of fruits with accelerometers. The resulting force is the three-dimensional vector result multiplied by the acceleration's derivative with time.

Tinoco et al. (2014) uses a heuristic process to identify the natural frequencies and modes of vibration on the fruit-peduncle system of Arabica coffee through modal analysis. The established criteria identify and define frequencies that produce rotation at the fruit-peduncle interface, obtaining ideal frequency ranges for harvesting ripe coffee.

Tinoco and Peña (2018) use the finite element method to analyze strengths in the Arabica coffee fruit-peduncle system. The study uses a frequency spectrum from 0*Hz* to 400*Hz* and discovered three vibration modes. The authors state that the natural frequency of the fruit decreases according to ripeness. The ideal vibration frequency for selective stripping is between 120*Hz* and 150*Hz*; this frequency range does not stimulate other ripening stages.

Examining acoustical applications in agriculture and its evolution is observed that the development of acoustic techniques applied to agriculture generates improvements and develops new methodologies. Precision agriculture demands the development of laboratory equipment, crop growing, and harvesting. Acoustical-based devices are already present in agricultural procedures, such as harvesting, ripeness evaluation, and computational harvest analysis (Adrian and Fridley, 1958; Brewer, 1965; Smith and Ramsay, 1983; Gomes et al., 2020).

Several studies apply acoustics as a tool in agriculture; however, there is a gap regarding vibration mode, currently obtained through direct contact with the plant. Controlled sound sources generate ambient pressure fluctuation, thus inducing vibration. The control of this vibration is through the frequency and power of the signal applied to the source. Controlling the induced vibration is feasible to reduce losses, increase crop productivity, develop laboratory procedures, and improve the quality of management and evolution in techniques. It is possible to remove fruits from their peduncles through vibration, and this harvest can be selective according to the frequency and amplitude of vibration. Therefore, it is possible to create methodologies using acoustically induced vibration to verify the behavior of the fruit while subject to vibration. Inducing vibrations directly in the fruit allows the analysis of oscillations, discarding the vibration obtained by the movement of the branch that generates an accumulation of kinetic energy.

The originality of this work is in the control that is performed in the sound sources through the frequency and power of the signal applied. Such sound sources generate pressure variation in the environment, inducing vibrations and the organized movement of suspended particles, enabling them to be directed, an essential factor in phytosanitary product applications. Induced vibration directly to the fruit allows laboratory procedures to evolve, reduce losses, increase crop productivity, and improve the quality of management and evolution in technique, defining the innovation of this research. Similitude processes are applied to evaluate the methodology, in which instrumented physical models are generated representing the fruits, enabling new practical studies on acoustics and vibration, frequency analysis, oscillation amplitude, and energy applied directly to the object under study.

The developed technique has intricated implementation due to sound source arrangement but uncomplicated control and data acquisition. The relevance and applicability of this work are according to agriculture needs to develop laboratory equipment for handling and harvesting. Primary hypothesis defines that if it is possible to remove fruits from their peduncles with vibration and with the correct frequency vibration and amplitude, it is feasible to have a selective harvest. Then it is attainable to create a methodology using acoustically induced vibration to develop selective harvesting equipment. Secondary hypothesis of this work defines that if sound pressure fields promote ordering in suspended particles, then sound pressure can be used to focus phytosanitary product pulverization.

In order to validate the hypothesis are developed methodology and devices. The acoustic and vibration techniques are applied in precision coffee production to reduce losses and increase productivity and product quality. Specifically: i) mathematical modeling of devices for inducing acoustic vibration, ii) similitude theory applied on the analysis of the direction of acoustic pressure, iii) laboratory system analysis of induced vibration, iv) selective coffee harvest technique using acoustically induced vibration, and v) focusing the application of phytosanitary products with controlled sound pressure fields.

2. Theoretical background

This session presents the theory for the execution of the project. It is divided into coffee harvesting techniques, phytosanitary products application, sound properties, modeling, and similitude.

2.1. Coffee harvesting techniques

In mechanical harvest, the coffee trees move through the machine, which has a rigid vibrating rod mechanism, which oscillates to obtain fruit detachment, as illustrated in Fig. 1, adapted from Queiroz et al. (2007).

These rods generate wear and tear on the plants and cause leaves to fall and break branches (Tavares et al., 2019). The operation mode and plant damage before and after harvest is illustrated in Fig. 2, adapted from Coelho et al. (2015).

Selective harvesting refers to only harvesting fruits that reach a specific quality or ripeness stage, preferably conducted within precise limits, avoiding harvesting green grains or advanced maturation stage. It is obtained as evolution of the traditional harvest machines based on vibrating rods (Zhang and Pierce, 2013).

For selective harvesting, the frequency, vibration amplitude, and the number of rods are controlled (Norris, 2001). This technique is highly complex due to several factors that influence the ideal vibration frequency, such as the ripeness stage, the number of fruits, and the size of branches (Queiroz et al., 2007; Tinoco et al., 2014).

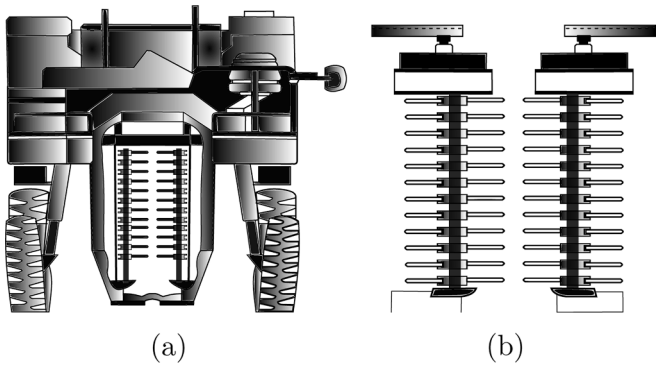

Fig. 1. Harvester: (a) front view of the harvest machine and (b) detail of the harvest mechanism.

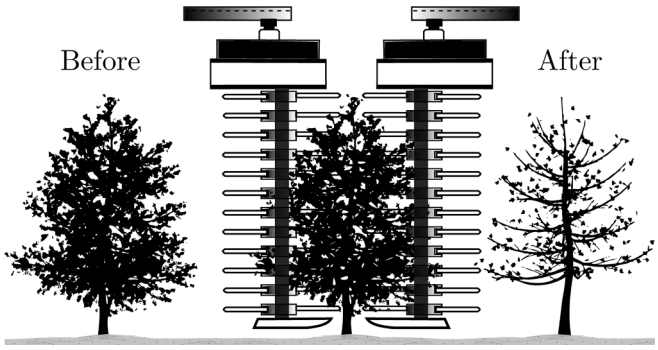

Fig. 2. Mechanical harvesting wear on the coffee tree.

2.2. Phytosanitary products application technique

The drift is the main problem associated with phytosanitary products pulverization. It is the dispersion of phytosanitary solution and occurs due to the spray diameter and weight, wind direction, and temperature. The drift causes evaporation, outpouring, displacement, increase production costs, and deposition of the phytosanitary product in undesired places, as shown in Fig. 3, adapted from Butts et al. (2019).

Fig. 3 illustrates two types of drift: i) endo-drift, which is the loss of the product within the cultural domains with outpouring caused by the abundance of product or incorrect spraying, and ii) exo-drift, which is the product loss outside the culture fields in which the spray drafts and evaporates. (Farooq et al., 2001).

Classical agricultural spraying techniques perform pulverization on the leaf top side; however, some diseases are located at the leaf bottom side (Baio et al., 2016). To reach the disease locus are developed methodologies such as: increasing the volume of product used, electrifying the drops, vortex pulverization, among others (Santinato et al., 2013).

The necessity to improve the accuracy of phytosanitary product application led to several studies such as i) high precision applications using micro jet applicators (Ivic et al., 2019; Salcedo et al., 2020), ii) drones for autonomous spraying (Faiçal et al., 2017; Meng et al., 2020; Ahmad et al., 2020), iii) variable rate application (Vondricka and Lammers, 2009) and iv) prompt weed detection using images (Blasco et al., 2002; Ahmad et al., 2018), among others.

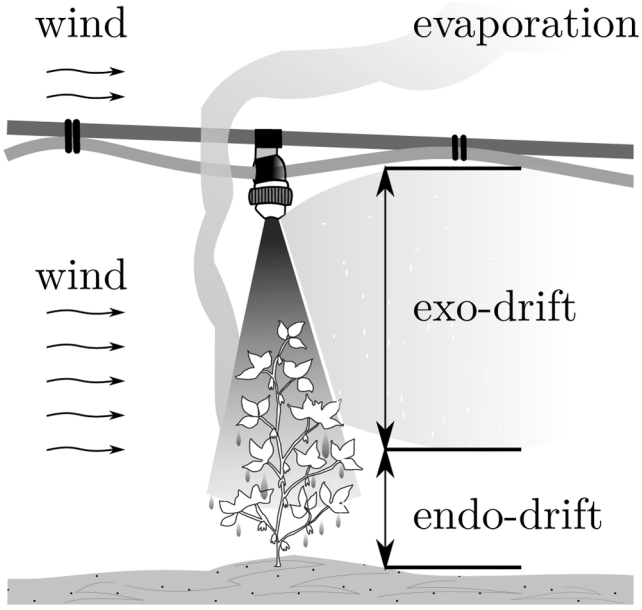

Fig. 3. Drift in agricultural spraying.

2.3. Sound Properties

Materials that react to a perturbation with noise are sound sources. However, acoustical studies require controlled sound sources. The primary controlled source is the electroacoustic transducer, transforming electricity into acoustic power. The conversion is executed by applying a controlled alternating current to the coils, generating a magnetic field, and producing transducer oscillation. This oscillation generates pressure variations and, consequently, sound waves (Kuttruff, 2006).

Acoustical sources radiate sound waves in all directions. In electroacoustic transducers, these waves are 180° out of phase. Therefore, when two sound waves are combined, they can cancel each other out, requiring isolation between two sides to prevent the acoustical short circuit (Beranek et al., 2012). Acoustic enclosures perform this isolation, operating as mechanical filters adjusted for constructive procedure (Ballou, 2013).

Particle displacement generated by sound can be measured as sound power level, SPL. Congruent and coherent sound sources can increase the SPL based on the delay between sound sources (Dunn et al., 2015). For two identical congruent sources, the resulting SPL will be $6dB$ higher than the individual (Beranek et al., 2012).

The average acoustic pressure analysis is related to distance variation, which led to the inverse square law relating to the decay of $6dB$ at acoustical power each time the distance from the source doubles (Kleiner, 2013).

The main characteristic of sound fields is that pressure changes are distributed throughout structure boundaries. The result of pressure variation relies on field properties, sound pressure, frequencies involved, sound level, phase, and the exposure time (Wilby, 2009).

Transmitting sound energy through the air between two media involves the vibration resulting in sound pressure in the first medium and the sound radiation in the second medium, causing a small transversal displacement of the structures. This process origin acoustically induced damage, studied primarily for the sound pressure generated by airplanes with jet turbines that damage structures involved (Fahy and Gardonio, 2007).

2.4. Similitude and modeling

It is necessary to understand the terms system, model, and simulation for design simulators. The system is the part of the real world that will be analyzed. Model is the mathematical or physical representation of this system (Rechtin and Maier, 2010). Simulation is the model analysis using input parameters to obtain results similar to the investigated system, based on a physical or mathematical model (Wainer and Mosterman, 2018).

The physical simulation performed using principles of scale reduction is called similitude. The similarity theory is the engineering field that studies the required conditions to establish similarities between phenomena. Similitude criteria assist in generating models correlated to other systems in which analyses are less complex than the originals (Coutinho, 2017).

When the initial parameters and conditions of material and geometric similarity are respected, the phenomena can be reproduced in prototypes of different scales with the equivalent evolution. The system determines which parameters are relevant and must be similar to both phenomena, which are irrelevant and discarded (Coutinho et al., 2018).

Szücs et al. (1980) classifies the study of similarity according to the parameters analyzed in: i) geometric similarity, in which the characteristics are equally staggered, ii) kinematic similarity, in which the characteristics are similar at similar times, and iii) dynamic similarity, in which similar parts of the system are subjected to similar forces.

Langhaar (1951) defines mathematically similitude as a function f' similar to f according to the constant ratio f'/f when evaluated in analogous situations. The ratio $\Lambda = f'/f$ is called the scale factor of the f function.

Westine et al. (2012) state that according to the achievement of similarity conditions, the models can be divided into: i) real model, in which all conditions are satisfied, and in this case, there is a complete similarity, ii) adequate model, the conditions related to the main parameters are satisfied, obtaining first-order similarity, and iii) distorted model, at least one of the main parameters is not satisfied, in this case, partial similitude is achieved.

Usually, only the first-order conditions are acknowledged, then the model used is adequate and their differences can be neglected (De Rosa et al., 2012). The ratio is determined by the definition of scale factor and relationship between parameters of prototype and model, as multiplicative factors of the chosen factor (Coutinho et al., 2016).

3. Material and methods

3.1. Acoustic system modeling

The electroacoustic transducer converts electrical energy into diaphragm displacement, producing a change in ambient pressure and sound. The speed of sound, ν, is determined by medium characteristic and waveform; therefore, it is related to temperature and the fluid it travels, expressed by (Shaw and Bugl, 1969):

$$\nu = (\gamma RT)^{\frac{1}{2}}[m{\cdot}s^{-1}] \tag{1}$$

Where γ is the specific heat rate, equal to 1.4 for air and other diatomic gases, T is the absolute temperature in Kelvin, and R, the specific gas constant. For air, it is equal to $R = 286.9[J/kg{\cdot}K]$

The acoustical modeling of the electroacoustic transducer is based on electrical and mechanical parameters defined by Albert Neville Thiele in the early 1960s (Thiele, 1971a; Thiele, 1971b), and improved by Richard H. Small in the early 1970s (Small, 1971; Small, 1972; Small, 1973). Known as Thiele-Small parameters, refer to the operation analysis and proposal to construct electroacoustic transducers and speakers. They are used to analyze the electroacoustic transducer, illustrated in Fig. 4, adapted from Beranek et al. (2012).

Fig. 4 illustrates the electroacoustic transducer. The voice coil has inductance L_e and resistance R_g, the diaphragm and wires of the voice coil have total mass M_{MD}. The diaphragm is mounted in flexible suspension in the center and at the edges. The effect of these suspensions gives rise to mechanical compliance C_{MS} and mechanical resistance R_{MS}. The front and rear parts radiate the sound. This radiation is called acoustic impedance radiation, represented as $Z_{AR} = 1/Y_{AR}$, where Y_{AR} is the acoustic admittance radiation. The mechanical radiation admittance analyzed on each diaphragm side is $Y_{MR} = S_D^2{\cdot}Y_{AR}$, where S_D is the effective area of the diaphragm, given by $S_D = \pi{\cdot}a^2$.

These parameters can be obtained from the device manufacturer datasheet; however, the production tolerance limits the direct application of the parameters in simulations. The acquisition of Thiele-Small parameters is performed using IEC 60268–5 standard (I. IEC, 2007).

The standard requires a quiet measurement location with a low reverberation index. The variable frequency source used must have an output impedance at least twenty times higher than the nominal impedance of the tested electroacoustic transducer. The value e_g is the value measured on the AC voltmeter before connecting the device to be analyzed. The parameters are measured as shown in Fig. 5, where $e_{g(rms)}$ is the *rms* voltage of the signal generator, R_g is the internal resistance of the signal generator and $e_{(rms)}$ is the *rms* voltage applied to the electroacoustic transducer.

The first parameter defined by Thiele-Small is the resonance frequency of the moving part of the transducer f_s, given by:

$$f_s = \frac{1}{2\pi\sqrt{M_{MS}{\cdot}C_{MS}}} \tag{2}$$

For the measurement of resonance frequency f_s, the applied frequency must be increased and simultaneously acquired the voltage between the electroacoustic transducer terminals. The maximum impedance corresponds to the maximum admittance. Consequently, the frequency that indicates the highest voltage between the terminals e_{max} is f_s.

After obtaining the value of f_s, the frequency is reduced until the voltage stabilizes, thus obtaining the lowest value in this measurement, e_{min}. With the voltage stabilized, the frequency is increased again until the voltage reaches $e_{mid} = \sqrt{e_{max}{\cdot}e_{min}}$, obtain f_L. Increasing frequency, until the value of e_{mid}, obtain the frequency f_U. From these values, the other Thiele-Small parameters are calculated in (3) quality of the mechanical part of the transducer, (4) quality of the electrical part of the transducer, and (5) total quality of the transducer.

$$Q_{MS} = \frac{f_s}{f_U - f_L}{\cdot}\left(\frac{e_g - e_{min}}{e_g - e_{max}}\right){\cdot}\sqrt{\frac{e_{max}}{e_{min}}} \tag{3}$$

$$Q_{ES} = \left(1 - \frac{e_{max}}{e_g}\right){\cdot}\frac{e_{min}{\cdot}Q_{MS}}{e_{max} - e_{min}} \tag{4}$$

$$Q_{TS} = \frac{Q_{ES}{\cdot}Q_{MS}}{Q_{ES} + Q_{MS}} \tag{5}$$

The total moving mass M_{MS} is calculated with the displaced air mass. Since $M_{MD} = M_{MS} - 2M_{M1}$ and $M_{M1} = 2.67a^3{\cdot}\rho_0$, the total moving mass is given by:

$$M_{MS} = \frac{1}{(2\pi f_s)^2{\cdot}C_{MS}} \tag{6}$$

The voice coil resistance R_E is measured with an ohmmeter and the effective diaphragm area S_d by direct measurement. The air volume displaced, V_{AS} is measured adding non-ferrous mass M_X to the diaphragm, which causes a change in the resonance frequency from f_s to f'_s, as given in (7). Thus, using mathematical representation, f_s as given in (2), and due to mass in motion change due to addition of mass M_X and with the aid of (6), obtaining the value of V_{AS}:

$$V_{AS} = \left(1 - \frac{f'^2_s}{f_s^2}\right){\cdot}\frac{S_D^2{\cdot}\rho_0{\cdot}\nu^2}{(2\pi f'_s)^2{\cdot}M_X} \tag{7}$$

According to Everest (2001), another essential parameter of the sound source is the acoustic power level, PWL, which is ten times the logarithm of the ratio between the acoustic power radiated by the source and the reference sound power ϖ_{ref}, usually $1pW$. When the sound source radiates $1W$ of acoustic power, it has a power level of $120dB$, as given by:

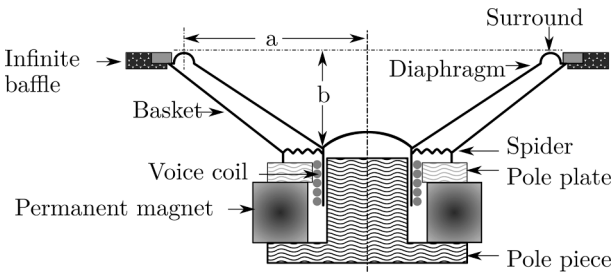

Fig. 4. Electroacoustic transducer construction diagram.

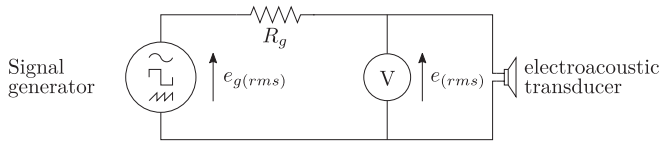

Fig. 5. Circuit used to determine Thiele-Small parameters.

$$\mathrm{PWL} = 10\log\left(\frac{\varpi}{\varpi_{ref}}\right)\left[dB\right] \tag{8}$$

The acoustical enclosure design is chosen from the resonance frequency values f_s in (2) and sound pressure level, SPL. The SPL is obtained through the measurement of effective sound pressure ρ_{rms} and the reference effective sound pressure ρ_{ref}, for general air measurements $\rho_{ref} = 20\mu\mathrm{Pa}$ *rms*, represented by:

$$\mathrm{SPL} = 20\log\left(\frac{\rho_{rms}}{\rho_{ref}}\right)\left[dB\right] \tag{9}$$

The sound intensity level, ILS, is ten times the logarithm of the ratio between the measured sound intensity and the reference intensity I_{ref}, usually $I_{ref} = 10^{-12}[W{\cdot}m^{-2}]$ in standard atmospheric condition, given by:

$$\mathrm{ILS} = 10\log\left(\frac{I}{I_{ref}}\right)\left[dB\right] \tag{10}$$

When the sound pressure level is high, the ambient pressure increases, inducing vibration. Particle acoustic direction is obtained by modifying the ambient pressure, steering the sound waves, and increasing the displaced airspeed.

For computational analysis, the constructive parameters of the enclosure type, internal volume, and size of the speaker duct are changed, causing changes in (i) sound pressure level, (ii) displaced airspeed, and (iii) apparent power provided by the amplifier.

After selecting the loudspeaker system, tests are performed to obtain the parameters related to the system angle following the IEC 60268–5 standard (I. IEC, 2007). The loudspeaker must be mounted $1m$ from the measurement point (location of microphones), as shown in Fig. 6. Directivity measurement is performed in intervals of 15° to the sound source center in the horizontal direction at different frequencies.

After the loudspeaker directivity individual measurement, the array directivity must be checked. The delay is calculated from the distances between the electroacoustic transducers, as illustrated in Fig. 7.

This analysis shows a change in intensity, sound pressure, and free space attenuation concerning the source distance, obtaining the graph of sound intensity by distance. The ideal delays of the arrangement are calculated from the central electroacoustic transducer, obtaining delays related to the time necessary for the sound waves from the different sources to reach the target point simultaneously, as illustrated in Fig. 8.

Calculating source delay requires: (i) sound speed in the middle ν, (ii) distance between centers of the electroacoustic transducers in vertical direction d_V and horizontal d_H and iii) distance relative to the target, which is positioned relative to the source at a distance d_{Ah} horizontally and d_{Av} vertically. Possessing differences of distances for each source is calculated the time necessary for the peak of the waves to reach the target simultaneously.

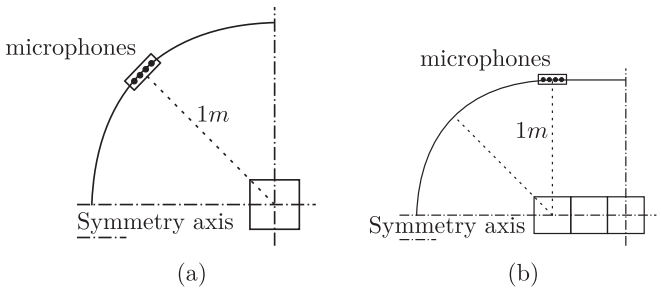

Fig. 6. IEC 60268–5 measurement: (a) single enclosure and (b) multiple enclosures.

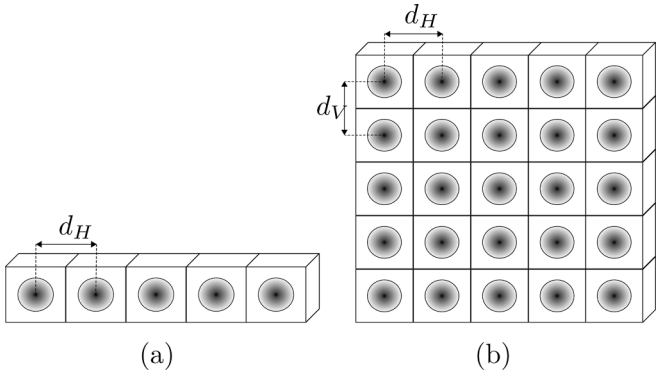

Fig. 7. Loudspeaker array: (a) One-dimensional and (b) Two-dimensional.

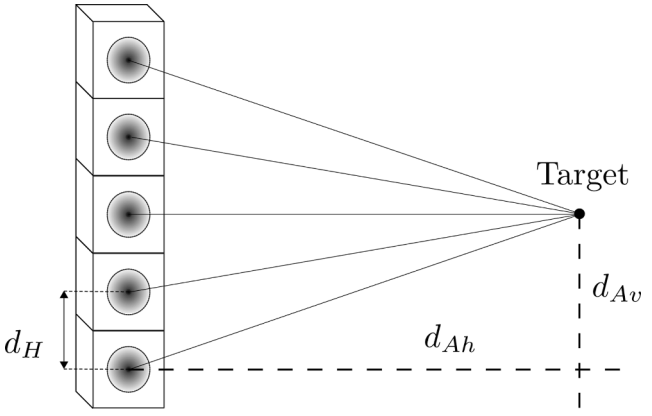

Fig. 8. Sound pressure direction through the sum of delays.

4. Design Requirement

This work developed prototypes in reduced scale and full scale. The main parameters of the project are analyzed in scaled-down prototypes to reduce the time and financial cost of full-scale prototyping.

After analyzing models on a reduced scale, a full-scale prototype is developed to perform tests. First acoustic vibration induction for selective harvesting, using an instrumented testing object, and second directing the application of phytosanitary products.

The parameters used for analysis are: (i) transducer radius, (ii) sound intensity *I*, (iii) sound pressure level *SPL*, and (iv) applied electrical power. The studies of these parameters were performed according to their basic units in the MKS system, reducing the number of parameters and enabling analysis of the scale factor for dynamic similarity. The scaled-down prototypes respect geometric and dynamic similarity criteria, enabling analysis of the prototype at full scale.

The full-scale prototype is developed similarly to the scaled-down model while respecting the electroacoustical transducer differences. The same acquisition system is used in the full-scale and reduced-scale prototype regarding the amplifier voltage and current differences.

The full-scale prototype uses different speakers to obtain the desired vibration and displacement at the point of highest sound pressure. Different frequencies are used to obtain the necessary displacement for the fruit to be detached. The proposed prototype induces vibration through the pressure oscillation generated by low and higher frequencies. The fruit to be harvested is the wave obstacle, thus delivering a higher vibration amplitude to induce oscillation in the fruit.

Both prototypes are composed of an audio amplifier, DC power supply, and electroacoustic transducers mounted in speakers. The acoustical enclosure is defined from the Thiele-Small parameters for the electroacoustic transducers. The sound pressure level and intensity

present a known scale factor Λ.

4.1. Acoustically induced vibration harvester

Parameter acquisition for monitoring the induced acoustic wear requires developing a data acquisition system to obtain the Thiele-Small parameters, directivity, and sound intensity. The acoustical force applied to the testing object and the array directivity is mathematically modeled using the acquired data.

The acquisition of the Thiele-Small parameters is performed using a current and voltage sensor, with a signal generation system, and applying the method described in Fig. 5. The applied force is measured from the body volume, mass, and displacement obtained through an accelerometer. The acoustic wear is measured using the applied force.

According to the required vibration amplitude, it is necessary to increase the delay between the wave peaks (maximum pressure) to increase the target vibration amplitude. Then the vibration is induced through two opposite wavefronts, congruent and out of phase.

Vibration is measured using accelerometers added to the target device, as illustrated in Fig. 9. The target device is developed in dimensions corresponding to coffee fruits. It can be related to the full-scale system concerning (i) resonance frequency analysis, (ii) acoustic induced vibration, and (iii) vibration modes and generated acoustic wear. Different assemblies are used to evaluate which combination of parameters: (i) waveform, (ii) frequency, and (iii) arrangement of the acoustical enclosures that obtain the best result.

The accelerometers are mounted in enclosures of known physical dimensions (surface area, total volume, mass, density, and center of mass) to accurately measure the acoustically induced vibration, as illustrated in Fig. 10. The fruit-peduncle force is calculated with these characteristics and the vibration, rotational or oscillatory, to which it is subjected.

The vibration is measured using accelerometers placed at the center of mass of the scaled prototype, as shown in Fig. 11. The body oscillation is measured, and the frequency and amplitude are acquired. The wear generated by the acoustically induced vibration is calculated from these parameters.

The constructive acoustical interference at congruent sound sources is generated in two ways: (i) fixed frequency, using the delay between loudspeakers, or (ii) different frequencies, focusing the highest sound pressure level on the scaled prototype. The sound directivity is measured with an array of microphones. It indicates the intensity and sound direction, obtaining a graph of sound directivity of the evaluated device.

In order to analyze the induced vibration for harvest, a prototype is built similar to the existing coffee harvester. Thus, to promote pressure variation and induce vibration in the prototype, a high sound energy density is required, obtained using electroacoustic transducers and high power amplifiers.

4.2. Acoustical vibration induction system for drift reduction

A high airflow acoustic enclosure is built for the analysis of phytosanitary products focusing. The pressure variation generated is directed towards the front of the speaker, allowing control over the application target, as it does not rely only on the directivity of the speaker.

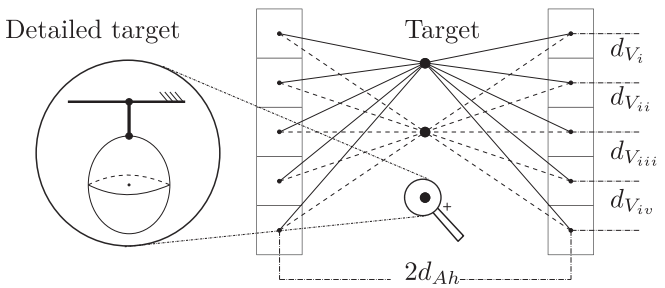

Fig. 9. Vibration induction simulator for acoustic harvesting.

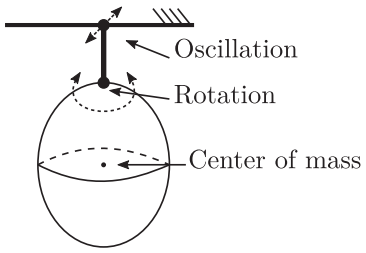

Fig. 10. Acoustically induced vibration on the scaled prototype.

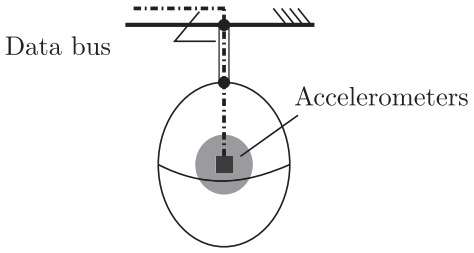

Fig. 11. Embedded sensors on the instrumented scaled prototype.

The application of the phytosanitary product is carried out using a backpack sprayer of 45*psi*, and the spray nozzle is connected to a sliding system with constant speed, obtaining uniform spraying in the test environment. The directivity is measured with hydro-sensitive paper, positioned at measuring points on the ground, with the sensitive part facing upwards and on tripods close to the ground with the sensitive part facing downwards, simulating the lower part of the plants. The concentrated application aims to reduce drift, and the spray nozzle must cross the entire area applying the phytosanitary product uniformly.

Fig. 12 and Fig. 13 illustrate application with moving sprayer and particles being directed acoustically. Fig. 12 shows that the spray nozzle moves on the application center line with constant spray displacement speed V_{dp}, allowing uniform application throughout the area (I.O. for Standardization-ISO, 2005). The influence of the pressure fields concerning the standard application is measured.

Fig. 13 presents the spray nozzle and the speakers move at a constant speed V_{dp}. In this way, pressure field action is measured across the entire application line.

4.3. Prototype validation

The prototype validation is obtained by comparing a mathematical model, a reduced scale model, and a full-scale model. An acoustic and electrical data acquisition device is developed to acquire the scaled-down and full-scale prototype parameters. The comparison between the mathematical model reduced models and built prototypes is based

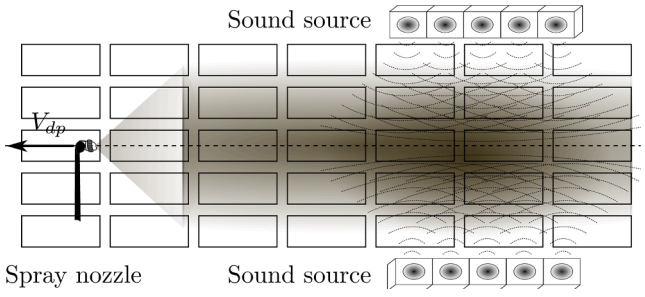

Fig. 12. Acoustically directed pulverization with dislocating spray nozzle.

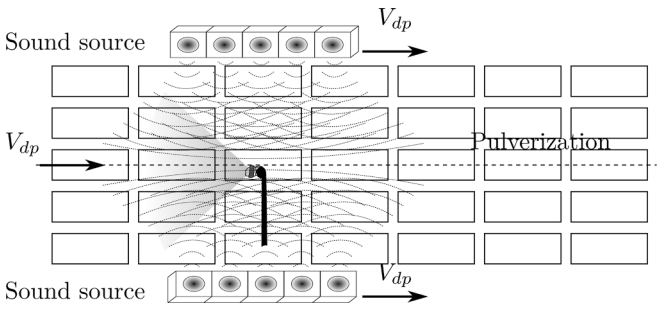

Fig. 13. Acoustically directed pulverization, speakers and spray nozzle in movement.

on parameters analyzed from impedance, resonance frequency, sound pressure level, and electrical power.

The acoustical focusing pulverization system is validated using backpack sprayer and hydro-sensitive paper, as illustrated in Fig. 14, in which the product is directed to the checkpoint P_4.

The prototype efficiency is measured by analyzing the amount of product that reaches the measurement points. Thus, the higher efficiency is obtained when the point P_4 has a higher percentage of coverage than P_2 and P_3. Interpreting the application in a real environment is equivalent to a product directed to leaf bottom, the biological target of the applications.

5. Results and discussions

5.1. Data acquisition system

The data acquisition system designed is shown in Fig. 15. The electroacoustic transducer is connected to the audio amplifier and the data acquisition module, respecting the device polarity, then signal generation is initiated. Following, the measurement of voltage and current characteristics of the electroacoustic transducer. The device impedance graph is generated from the measured values. Analyzing the curve is obtained the Thiele-Small parameters of the electroacoustic transducer.

Acoustical data acquisition systems rely on environmental factors such as temperature, humidity, and atmospheric pressure. Therefore, these parameters must be evaluated to develop the data acquisition system. The ambient temperature and humidity parameters are obtained with a temperature measurement range from -40 °C to 125 °C with an accuracy of ± 0.5 °C and humidity between 0% and 100% with an accuracy of 2%. The pressure is measured with a range of 300 and 1100hPa with an accuracy of 0.02hPa, equivalent to 0.17m of variation.

The data acquisition module is started remotely, and the first test performed is the audio interface connection, verifying the number of audio outputs and channels available. Then, the sensors and initial readings of voltage, current, temperature, pressure, and humidity. At this moment, the initial environmental parameters to calculate the

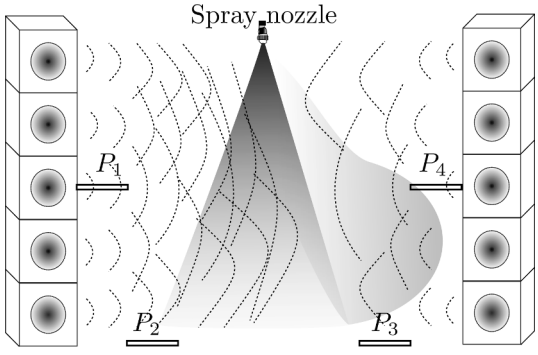

Fig. 14. Phytosanitary product focusing validation.

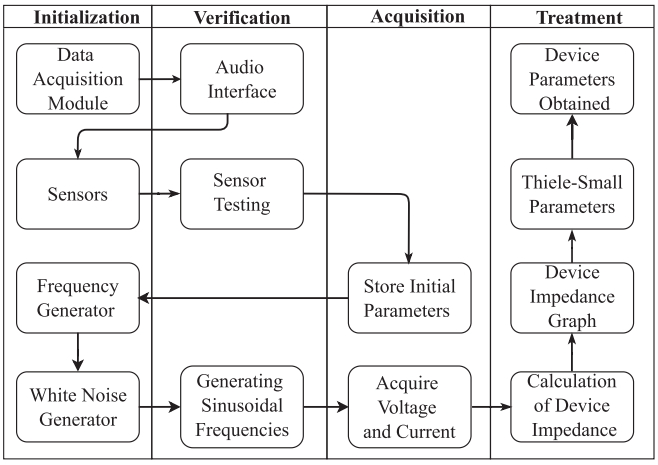

Fig. 15. Data acquisition system.

sound speed are stored.

The project uses two audio amplifiers selected according to electrical power. Scale reduction studies are performed with low power, the amplifier with two output channels of 5V and DC power of 3W. For the full-scale prototype, amplifiers of 1000W and 1600W are used, with a 12V DC power supply.

The frequency generator is started and tested with white noise for ten seconds to check and adjust the electroacoustic transducer voltage to 1V. Then, start the frequencies generation from 10Hz to 7.5kHz and simultaneously acquire voltage and current for each frequency. With the frequency, current, and voltage data, it is calculated the impedance for each frequency. Finally, the device impedance graph is generated, as shown in Fig. 16, and the Thiele-Small parameters are obtained from the analysis of the impedance graph, as shown in Table 1.

5.2. Full-scale prototype

The full-scale prototype is developed from the analysis of the parameters of the electroacoustic transducers. Specifics acoustical enclosures are designed for each transducer. The enclosure design limitation is related to the dimensions of the transducer used; however, enclosures above 0.10m^3 are not feasible due to their weight and large dimensions.

The prototype has three amplifiers, two of 1000W and one of 1600W, a battery bank with four batteries of 12V and 150A parallel connected, a capacitive filter of 5F, as shown in Fig. 17. The amplifier is used in

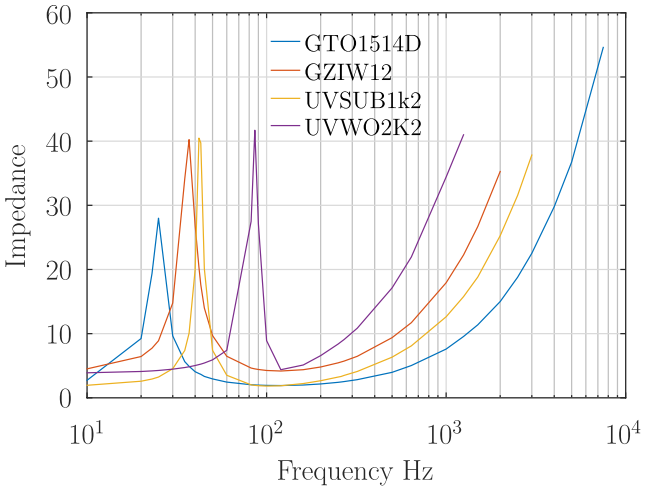

Fig. 16. Impedance graph for the electroacoustical transducers used on the full-scale prototype.

Table 1
Thiele-Small parameters of electroacoustic transducers used on the full-scale prototype.

Producer	Ultravox		Ground Zero	JBL
Model	UVWO2k2	UVSUB1k2	GZIW12	GTO1514D
Diammeter [mm]	284	285	310	345
Power [W]	2200	1200	700	350
F_s [Hz]	79,59	42,44	36,90	24,90
Q_{TS}	0,75	0,67	0,67	0,47
Q_{ES}	0,81	0,70	0,75	0,51
Q_{MS}	10,43	16,19	6,57	7,15
V_{AS} [l]	15,17	17,92	35,60	161,40
R_e [Ω]	2,80	1,80	4,10	1,90
BL [Tm]	13,33	12,35	16,1	12,08

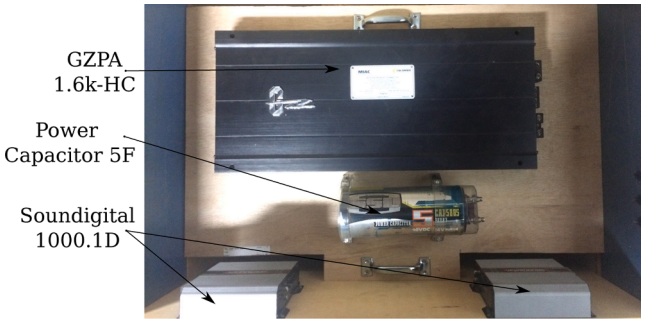

Fig. 17. Audio Control Panel.

electroacoustic transducers and tested in a fourth-order bandpass box and a second-order bandpass box.

In Fig. 17, the wires and connections were removed so as not to pollute the image. The main difference between both is the presence of ducts on the front and rear part of the acoustical enclosure, the fourth-order bandpass, enabling higher airflow and high acoustic power in a narrow operating range.

The full-scale prototype is developed using 20 electroacoustic transducers. The final assembly is 2.40m height and 1.60m width, having dimensions based on commercial coffee harvesters. The prototype is shown in Fig. 18, and the characteristics of each acoustic source are presented in Table 2.

Fig. 18 presents the assembly of the prototype using: i) eight bandpass boxes used for the transducer that is connected to the amplifier of 1600W, ii) eight sealed boxes used for the transducer, connected to the 1000W amplifier, and iii) six bandpass enclosure.

5.3. Acoustical array and steering

Congruent sound sources allow an increase in the sound intensity due to obtaining constructive wave interference. In order to generate these waves is used a calculated phase delay, referring to the target point.The calculation is performed for a single frequency, then the following frequencies that obtain the peak at the same point are checked. The wave peak is directed to the midpoint between the sources, adjusted according to the necessity of changing frequency.

The sound source distance defines the frequencies required to focus on points of maximum pressure, called hot spots. In which, for speed of sound, $\nu = 343ms$ and distance between the source and the target of 2.0m, we have that the first five frequencies that reach the peak pressure on the target are: i) 42,875Hz, ii) 214,38Hz, iii) 385,88Hz, iv) 557, 38Hz and v) 728, 88Hz, as shown in Fig. 19.

The delay is generated mathematically concerning the distance between the sources and the target. The sound speed is calculated online for the environment, considering ambient temperature and atmospheric pressure. The audio vector is generated with the necessary delay for each

Table 2
Acoustic source characteristics.

Acoustic Source	4^{th}	A.2^{nd}	$B.2^{nd}$	$C.2^{nd}$
Eletroacoustic Transducer	Ground Zero GZIW 12”	Ultravox UVSUB1k2 12”	JBL GTO1514D 15”	Ultravox UVWO2k2 12”
Power rms [W]	700	1200	350	2200
Power Peak [W]	1000	2400	1400	4400
Frequency response [Hz]	35–120	20–1700	23–400	50–3000
Type	Bandpass 4th order	Vented	Vented	Vented
Volume	V1: 21L/ V2: 35L	40L	55L	35L

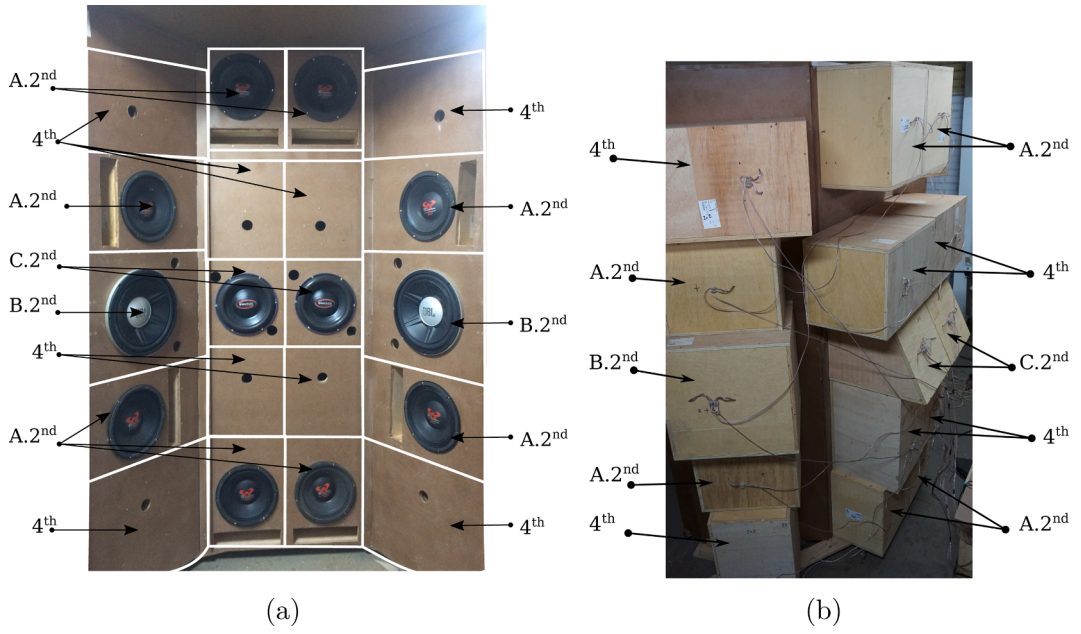

Fig. 18. Acoustical enclosures in full-scale prototype: (a) front view and (b) rear view.

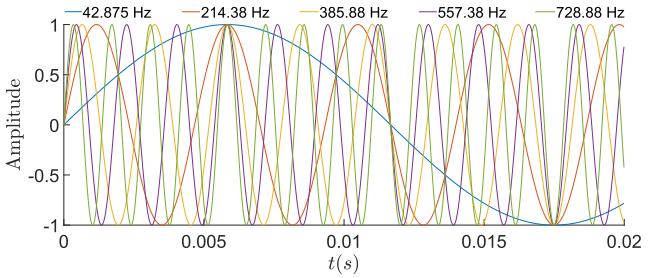

Fig. 19. Acoustical enclosure array.

sound source, and each audio vector is directed to the specific channel of the scaled-down model. This data is generated using an audio card and amplifier, obtaining two output channels per set.

The sound pressure gain is obtained using congruent sound waves generated through delays for focusing the sound pressure. The delay is calculated from the center of the array. The direction obtained is verified with microphones and an SPL meter.

The arrangement is rotated by 15° with each measurement, with a microphone at a distance of one meter. This pressure gain is evaluated in scale reduction, with 25 sound sources. Different arrangements are assembled and polar graphs are generated indicating the direction obtained: i) 3 × 3 shown in Fig. 20(a), ii) 4 × 4 shown in Fig. 20(a), and iii) 5 × 5 shown in Fig. 20(c). Table 3 presents the directivity analysis of the array, indicating the maximum intensity and dispersion.

Fig. 20 shows an increase in directivity with an increase in frequency. Acoustical enclosures array obtain the same pattern by increasing the number of acoustical sources, obtaining a higher directivity.

The array can be linear, as shown in Fig. 21, which presents the result of the array of 3, 5, 7, and 9 acoustical enclosures to obtain a uniform and single front wave using a frequency of 250*Hz*. Table 4 presents the directivity analysis of the array, indicating the maximum intensity and dispersion.

Fig. 21 shows the linear arrangement of sound sources. The polar graph analysis shows an increase in directivity related to the number of transducers in the array.

5.4. Phytosanitary product targeting

A phytosanitary product application is performed with a backpack sprayer with an operating pressure of 45*psi*. The application is carried out in an wind-free environment. An electroacoustic transducer mounted in a specific acoustic enclosure promotes high flow and air and direction of sound fields.

The case study on the targeting of the phytosanitary product represents the leaf coverage test. The spray nozzle is a full cone, positioned at

Table 3
Dispersion analysis of the array.

Number of Elements	Dispersion	50 Hz	250 Hz	500 Hz
3 × 3	Array Directivity	4.80 dBi	5.38 dBi	7.19 dBi
	Azimutal	131.00°	115.00°	81.96°
	Elevation	132.00°	116.00°	82.00°
4 × 4	Array Directivity	4.82 dBi	5.91 dBi	9.10 dBi
	Azimutal	129.00°	103.02°	64.24°
	Elevation	130.00°	104.00°	66.00°
5 × 5	Array Directivity	4.84 dBi	6.58 dBi	11.12 dBi
	Azimutal	130.00°	92.00°	54.00°
	Elevation	129.00°	90.76°	52.28°

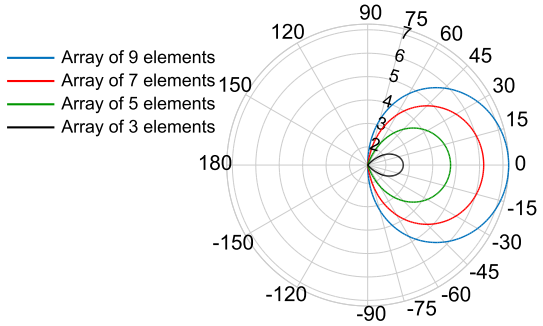

Fig. 21. Linear array directivity.

Table 4
Linear array directivity at 250 Hz.

Number of Elements	Array Directivity	Dispersion	
		Azimutal	Elevation
3	8.06 dBi	47.10°	132.00°
5	10.08 dBi	28.02°	132.00°
7	11.49 dBi	19.94°	132.00°
9	12.56 dBi	15.48°	132.00°

0.60*m* height, with the hydro-sensitive papers separated by 0.15*m* horizontally and 0.20*m* vertically. The hydro-sensitive paper has the function of simulating the leaves. It is positioned in the test area as shown in Fig. 12 and Fig. 13. The first test performs pulverization with the spray nozzle in motion. The loudspeakers are placed next to the column **6** to focus the application. The results of the application are shown in Fig. 22 and the numerical analyses in Table 5.

Fig. 22 shows the water-sensitive papers collected after the spraying procedure. The analysis of the direction of the phytosanitary product using sound pressure fields focusing pulverization on the column **6**. The number of darker points indicates points where the paper gets in contact

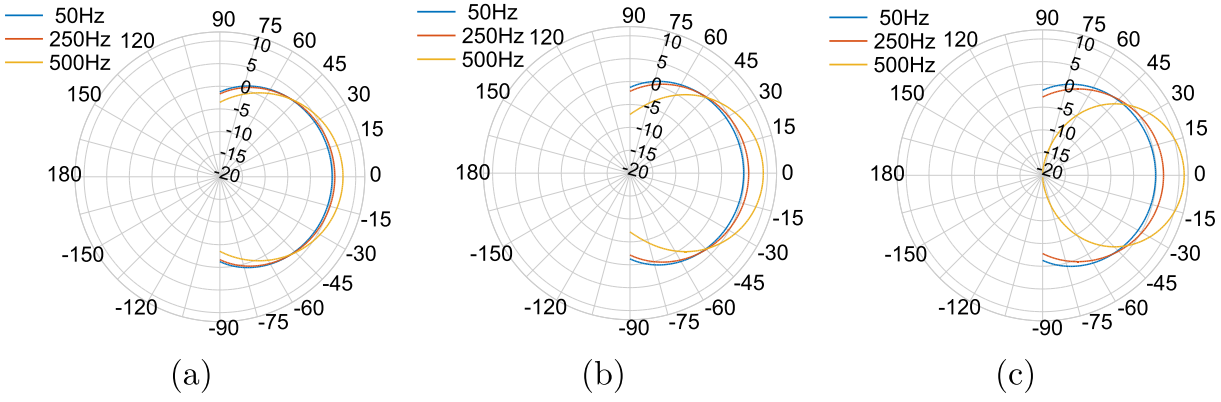

Fig. 20. Quadratic arrangement direction at frequencies of 50*Hz*, 250*Hz* and 500*Hz* measured in: (a) 9 sound sources, (b) 16 sound sources, (c) 25 sound sources.

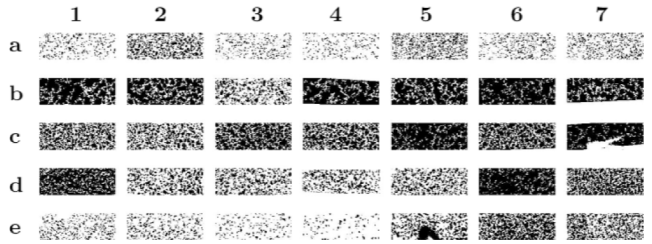

Fig. 22. Collumn pulverization focusing.

Table 5
Percentage of foliar coverage for column targeting of the Fig. 22.

	1	2	3	4	5	6	7
a	12.16	32.82	11.90	9.23	27.38	14.89	18.87
b	78.34	72.00	29.84	76.32	74.85	85.59	66.61
c	49.47	39.53	66.48	56.41	84.49	61.42	72.09
d	75.51	33.86	31.14	28.08	32.76	86.04	57.70
e	16.35	16.75	9.29	6.30	39.31	57.94	40.80

with the phytosanitary product.

The hydro-sensitive papers from the column **6** show that leaf coverage is higher than in the other regions. It is also verified that the pulverization without focusing, in columns **1** to **5** and **7**, has a higher dispersion rate, resulting in a higher drift of the phytosanitary product.

In the second test, the spray nozzle and the loudspeakers move uniformly alongside the application plane, focusing the application in lines **c** and **d**. The application results are shown in Fig. 23, and the numerical analysis in Table 6.

Fig. 23 shows the water-sensitive papers collected after the pulverization procedure. The directivity analysis of the phytosanitary product using sound pressure fields focuses the application on lines **c** and **d**. The percentage of leaf coverage is represented in the image from the number of darkened points, which indicate the points the paper enters in contact with the phytosanitary product.

By relating the average leaf coverage presented in Table 5, the lines **b**, **c**, and **d** in the columns without focusing, columns **1** to **5** and **7**, a mean coverage of 62.09% is obtained. The average of column **6**, lines **b**, **c**, and **d**, in which the application is focused using the proposed technique, obtain a mean coverage of 85.59%. The increase in leaf coverage from 62.09% to 85.59% represents an efficiency increase of 37.85%.

The focusing efficiency of the in-line proposed technique is obtained through the average leaf coverage on lines **c** and **d** of Table 6, obtaining a coverage value of 80.52% with the proposed focusing method, related to the average values of leaf coverage on lines **c** and **d** of Table 5 at columns without direction, columns **1** to **5** and **7**, that obtain a value of leaf coverage of 52.94%. The increase in leaf coverage from 52.94% to 80.52% represents an efficiency increase of 52.10%.

The analysis shows that the leaf coverage is higher in lines where the application is focused than in the other regions. Analyzing the first experiment, with an increase of 37.85%, and the second experiment, with an increase of 52.10%, is obtained an average increase of 44.97% in leaf coverage with the proposed technique.

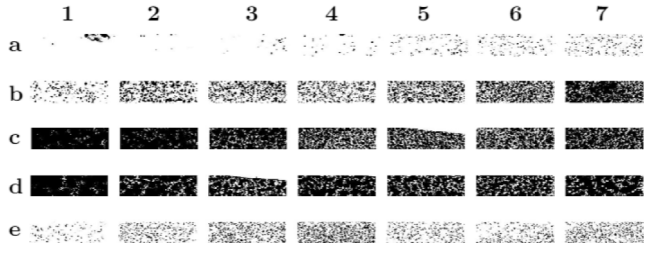

Fig. 23. Line pulverization focusing.

Table 6
Percentage of foliar coverage for line focusing of the Fig. 23.

	1	2	3	4	5	6	7
a	4.19	0.41	1.29	2.46	5.23	5.92	7.71
b	13.18	33.62	34.39	26.56	39.91	52.04	77.74
c	97.22	94.79	84.80	64.76	60.10	63.63	77.46
d	95.85	87.08	67.80	83.46	77.59	77.21	84.28
e	4.75	14.11	24.39	31.58	13.88	12.13	19.69

In order to verify the drift reduction lines **a** and **e** from Table 6, with an average of 6.81%, and lines **a** and **e** from Table 5, at columns without direction, columns **1** to **5**, and **7**, with an average of 16.55%, are compared. The drift rate dropped from 16.55% to 6.81%, representing a reduction of 58.82% of drift, proving increasing directivity and drift reduction, improving the efficiency and efficacy using the proposed method.

The performance increase is due to the direction produced by the controlled airflow by the electroacoustic transducers, which produces displacements at points of higher sound pressure. The sound pressure variation induces directivity through pressure oscillation generated by low and high frequencies, thus providing a greater amplitude of leave coverage.

5.5. System model validation

The validation is performed in two steps: (i) simulated coffee bean and (ii) real coffee bean. The first uses the similitude method to analyze the acoustic force applied to the model and the vibration method. The second method uses the full-size model with coffee branches in the laboratory to obtain quantitative harvest results.

5.5.1. Simulated coffee bean

The simulation project uses measuring instruments, signal generation, amplifiers, electroacoustical transducers, and acoustic enclosures. These devices are arranged in Table 7. The characteristics of the electroacoustic transducers used are shown in Table 1.

The vibration is measured with the accelerometer MPU9250, connected via an I2C interface to a Raspberry Pi board. A decibel meter with

Table 7
Devices used in the project.

Device	Application	Datasheet
MPU9050	Inertial sensor	(MPU-9250 Product Specification, 2016)
DHT22	Temperature and humidity sensor	(Temperature and humidity module - AM2302 Product Manual, 2015)
BMP280	Pressure sensor	(BMP280 - Digital Pressure Sensor, 2021)
Raspberry Pi 3B+	Control board	(Raspberry Pi 3 Model B+, 2018)
GZPA 1.6 HC	Audio Amplifier	(Ground Zero Plutonium GZPA 1.6K-HC Owner's Manual, 2015)
Soundigital 1000.1D	Audio Amplifier	(Instruction Manual SD1000.1D, 2015)
Ground Zero GZIW 12"	Subwoffer	(GZIW 12 SPL, 2017)
Ultravox 1k2 12"	Subwoffer	(Ultravox - Shocker Terremoto 1k2, 2015a)
JBL GTO1514D	Subwoffer	(Grand Touring Series - GTO1514D, 2012)
Ultravox 2k2 12"	Woffer	(Ultravox – Pancadão 2k2, 2015b)
Loudspeaker 3 W 4ohm	Full range	N.A.
PAM8403	Audio Amplifier	(PAM8403 Filterless 3W Clas-D Stereo Audio Amplifier, 2012)
USB Soundboard	Audio Interface	N.A.
Shure SM58	Microphone	(Shure S58 User Guide, 2006)
Behringer X1204USB Xenyx	Audio Interface and controller	(XENYX X1204USB - User Manual, 2021)

a measurement capacity of 30dB to 130dB, resolution 0.1dB, frequency response 31.5Hz to 8.5kHz, manufacturer Minipa, model $MSL-1355B$ is used. It was developed a control and acquisition board, with signal generation and control for verification of the Thiele-Small parameters according to Fig. 15. The measurement of atmospheric pressure was performed using the BMP280 sensor, temperature and humidity using the DHT22 sensor, and a microphone to verify the sound directivity.

The simulated coffee bean uses an instrumented device with an MPU9250, an accelerometer, and a gyroscope sensor, as shown in Fig. 24(b). The data is analyzed to obtain the vibration amplitudes of the simulated coffee bean, oscillations, and indicate the acceleration. The position in time is obtained by applying double integration on the acceleration signals.

Fig. 24(a) displays the target project, and Fig. 24(b) shows the 3D-printed instrumented target. Fig. 24(c) shows the small scale prototype with a quadratic array of sixteen loudspeakers. Each electroacoustic transducer has a diameter of 50mm and a power of 3W. The Fast Fourier Transform is applied for each of the three dimensions and calculates the resultant vector to obtain the vibration direction. The values of intensity and direction oscillate due to the sound source frequency and ambient damping. The vibration modes are presented in Fig. 25.

Fig. 25 present the movement induced by the sound source to the simulated coffee bean. Each frequency generates different displacement, such as: i) oscillatory with 72Hz, 52Hz, and 45Hz, in which the target moves in one direction, ii) rotational with 42Hz and 24Hz in which the target moves in two different directions and iii) oscillatory and rotational with 18Hz and 12Hz. The movement amplitude indicates more significant displacement in the grain; however, a greater amplitude (frequency of 72Hz) does not imply a greater harvest rate. The harvest rate depends on a more substantial oscillatory and rotational motion, ideal for grain harvesting without the peduncle.

5.5.2. Real coffee bean

The real-size model is lab-tested with coffee branches to harvest beans in the proper state of ripeness. Fig. 26 presents the experimental test with details of the coffee beans before and after harvesting by acoustic induction. For the analysis of the proposed methodology, coffee tree branches with leaves (plagiotropic lateral branches) were used. Three stages of fruit maturation were considered: i) green fruits ≈ 15%, ii) ripe fruits (adequate) ≈ 60% and ii) dried fruits ≈ 25%. A stripping rate of ≈ 40% was obtained for fruits at the appropriate ripening stage and ≈ 10% for green and dry grains, ensuring the desired precision in carrying out the selective harvest.

The coffee tree branch was cut carefully to not detach the fruit in the field. For transport from the field to the laboratory, it was necessary to cover the branch in silicone fiber to reduce fruit detachment. For the selective stripping, the frequency of 18Hz was used in the grains. However, to obtain 18Hz in the grains it was necessary to impose 42Hz on the electroacoustic transducers 4^{th}, $A.2^{nd}$ and $B.2^{nd}$ and 557Hz on the electroacoustic transducers $C.2^{nd}$ (Fig. 18 and Table 2). These frequency values are seen in Fig. 19.

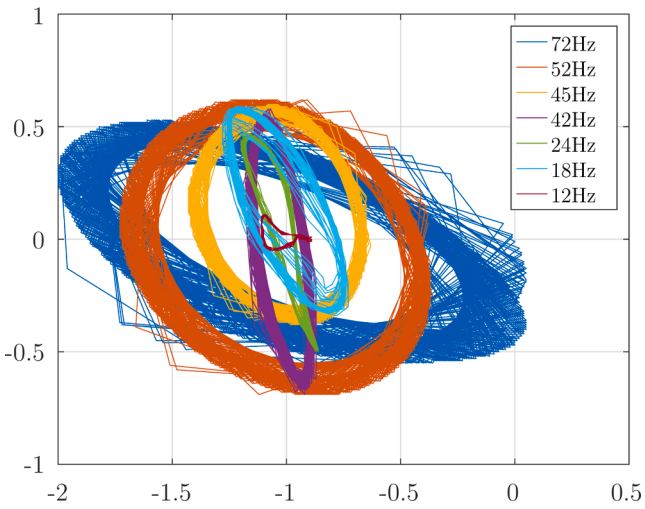

Fig. 25. Small scale analysis of grain vibration.

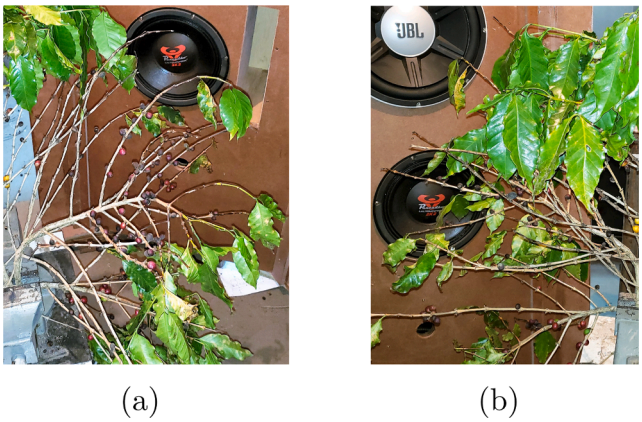

Fig. 26. Acoustical harvest laboratory tests with coffee branches: (a) before and (b) after.

5.6. Discussion

Acoustic techniques applied in agriculture are limited to reducing vibrations and sound noise, aiming at operator comfort, and reducing machine wear. In this work, acoustic techniques are applied to assist in: i) directing the application of the phytosanitary product, reducing drift and obtaining a better percentage of leaf cover, and ii) inducing vibrations in a controlled manner, without contact with the plants and

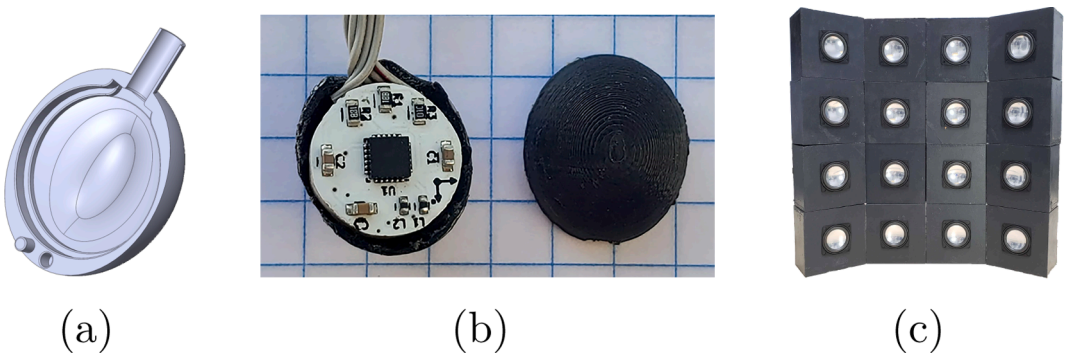

Fig. 24. Instrumented target: (a) project for 3D printing, (b) printed target with encapsulated inertial sensor (MPU9250) and (c) small scale quadratic prototype.

performing selective harvest.

The application of the techniques proposed in this work to agriculture has the potential to improve agricultural development due to the reduction of the amount of phytosanitary product used, reduction of losses due to the inherent wear of the traditional harvest method, and increase in the aggregate value of the grain due to selective harvesting.

Traditionally, the targeting of phytosanitary products is obtained through an air barrier or electrification of drops (Farooq et al., 2001; Jørgensen et al., 2007; Baio et al., 2016; Santinato et al., 2013). According to Balsari et al. (2007), air induction nozzles can reduce drift to an average of 6.80%, proving the accuracy of the proposed methodology, which obtains an average drift of 6.81%. Traditional techniques do not allow application in adverse environmental conditions. In this work, the application targeting is obtained with the variation of sound pressure, allowing targeting according to the positioning of the biological target in the plant. Another critical factor is the acquisition of environmental parameters, analyzing these variations in the calculations used for targeting. If there is a change in the wind direction, the sound pressure direction can be changed to compensate for the ambient changes.

Another point addressed in this work is the application of acoustic similitude, scale reduction methods to create, analyze and validate acoustic techniques. Acoustic studies are generally based on simulations of finite element methods, but the complexity of the simulation limits its use (Karjalainen et al., 2001; Ahonen, 2003; Sahu et al., 2015; Bezzola et al., 2019). The results obtained in scale reduction allow making inferences about the measurements of the full-size prototype with the ease and precision of instruments used on the bench and reducing the financial cost and time required for the construction and testing of the devices.

The application of vibration for harvest is a recurrent practice in agriculture. Several works that analyze this technique are based on the existing technology of vibrating rods in contact with the plant. Studies for the evolution of the technique are limited to the analysis of frequency and amplitude of vibration of the rods to perform selective harvest. Laboratory bench analyses are based on direct vibration transmission, in which the branch is connected to a controlled oscillating platform, and the ideal values for stripping are based on the accumulation of kinetic energy (Norris, 2001; Tavares et al., 2019; Queiroz et al., 2007; Júnior et al., 2020). This work obtains the vibration frequency for harvest by analyzing the vibration mode and induced oscillation without contact directly in the fruit.

Compared with results from Silva et al. (2015) and Kazama et al. (2021), which present efficiency in selective harvest from 72% to 92%, highly related with the harvest time. This work presents a new technology that is on prototype phase and performs selective harvest without contact to the plant; still, it has already been achieved an efficiency of approximately 40% and causes no wear to the plant, justifying the lower efficiency when compared to others commercial techniques.

During the development of this work, difficulties arose such as (i) necessity of specific equipment to measure the mechanical and electrical parameters of the system, requiring the construction of different types of equipment to perform the studies and (ii) short harvest period on the farm that supplies the grains, limiting the time for adjusting the technique and testing the devices developed. Some errors were overcome, such as (i) use of transducers with an incomplete description of the manufacturer and incorrect parameters, (ii) construction of loudspeakers using the parameters provided by the manufacturer and not with real device parameters, (iii) amplifiers that need post-treatment to reduce noise, (iv) tests performed with grains outside the ideal harvest period and (v) tests performed using the vibration frequency indicated for traditional harvesting.

In this work, several results with the potential application were achieved, such as: (i) wavefronts to increase the sound pressure, (ii) direction of the sound pressure from the frequency variation, (iii) difference of the induced movement according to the type of waveform used, (iv) use of scale reduction techniques to perform tests outside the harvest period, (v) scale reduction to evaluate the direction and acoustic parameterization, (vi) verification of environmental parameters to obtain sleep speed in the environment, increasing accuracy in acoustic applications and allowing tests in different environmental conditions and (vii) use of microphone array to verify sound direction.

The proposed methodology is a technique under development whose time for field analysis is limited to the harvest period. In the laboratory, the methodology presented is promising since part of the grains with an adequate degree of maturation are detached during transport from the field to the laboratory; still, an average rate of $\approx 40\%$ was obtained in the selective stripping. It is expected that field tests will reach values of around 65% for harvesting grains with an adequate degree of maturation.

Table 8 provides a summary of the selective harvest performed on the branch transported from the field to the laboratory, shown in Fig. 26. It was observed that: individual delays in the full-scale prototype should be used to measure vibration in field tests. In addition, tests should be avoided in some circumstances such as i) closed environments due to the influence of sound pressure on the human body, ii) tests with incorrect power supplies and use of transducers above the rated power, and iii) adaptation of speakers without performing software tests as impedance changes may cause damage to the device.

6. Conclusions

The primary purpose of this work is the development and application of acoustic techniques to precision coffee growing. The work proposes the development of a prototype to perform the targeting of phytosanitary products to be applied using an orderly flow of air and vibration and a selective coffee harvest system without contact with the plant.

To develop the research, electrical and acoustic data acquisition systems are produced to analyze the prototypes before their construction. The acoustic enclosure design is based on the parameters acquired and validated for the electroacoustic transducer, and the mechanical characteristics are analyzed by software. The vibration induction simulator is built for both applications, phytosanitary products and selective coffee harvest, allowing analyzing the control over the variables and the precision in the measurements. With the validated simulator, using similarity techniques, instrumented prototypes are developed. The prototype for the application of phytosanitary products is built, and results are obtained of drift reduction and increase in leaf coverage. Through the acoustic induction vibration prototype for selective harvest, the vibration mode obtained by different frequencies is analyzed, making it possible to use the frequency of $18Hz$ in the grain for selective stripping.

The analysis carried out in this work presents arguments that accompany the literature when observing the fruit vibration at a frequency of $18Hz$. However, to generate this vibration directly in the coffee bean, it is necessary to induce high frequency, in the range of $42HZ$ to $557Hz$. The work also proposes the use of variable frequencies in order to direct the pressure beam, obtaining the highest sound pressure directly on the fruit, which is the target of selective stripping. Therefore, it is concluded that the proposed methodology can be used in precision agriculture, since it obtained a reduction in drift and an increase in leaf cover on average of approximately 44% and it was still possible to carry out the selective stripping with approximately 40% of

Table 8
Summary of the application of selective stripping in the laboratory.

	Maturation stage		
	Green	**Cherry**	**Dry**
Distribution	15%	60%	25%
Harvest rate	3%	40%	7%

efficiency.

Declaration of Competing Interest

The authors declare that they have no known competing financial interests or personal relationships that could have appeared to influence the work reported in this paper.

References

Beranek, L.L., Mellow, T.J., 2012. Acoustics: sound fields and transducers. Academic Press.

Dunn, F., Hartmann, W., Campbell, D., Fletcher, N.H., 2015. Springer handbook of acoustics. Springer.

Desmet, W., Pluymers, B., Sas, P., 2003. Vibro-acoustic analysis procedures for the evaluation of the sound insulation characteristics of agricultural machinery cabins. J. Sound Vib. 266 (3), 407–441.

Escola, J.P.L., Guido, R.C., da Silva, I.N., Cardoso, A.M., Maccagnan, D.H.B., Dezotti, A. K., 2020. Automated acoustic detection of a cicadid pest in coffee plantations. Comput. Electron. Agric. 169, 105215.

Gorthi, S., Chakraborty, S., Li, B., Weindorf, D.C., 2020. A field-portable acoustic sensing device to measure soil moisture. Comput. Electron. Agric. 174, 105517.

Ebrahimi, R., Esfahanian, M., Ziaei-Rad, S., 2013. Vibration modeling and modification of cutting platform in a harvest combine by means of operational modal analysis (OMA). Measurement 46 (10), 3959–3967.

Tang, Y., Dananjayan, S., Hou, C., Guo, Q., Luo, S., He, Y., 2021. A survey on the 5G network and its impact on agriculture: Challenges and opportunities. Comput. Electron. Agric. 180, 105895.

Parchomchuk, P., 1971. Vibratory fruit harvesting: An experimental investigation of an apple fruit-stem response to forced oscillations. Cornell University.

Cooke, J., Rand, R., 1969. Vibratory fruit harvesting: a linear theory of fruit-stem dynamics. Journal of Agricultural Engineering Research 14 (3), 195–209.

Rand, R., Cooke, J., 1970. Vibratory fruit harvesting: a non-linear theory of fruit-stem dynamics. Journal of Agricultural Engineering Research 15 (4), 347–363.

Parchomchuk, P., Cooke, J.R., 1972. Vibratory harvesting: an experimental analysis of fruit-stem dynamics. Transactions of the ASAE 15 (4), 598–0603.

Tsatsarelis, C., 1987. Vibratory olive harvesting: the response of the fruit-stem system to fruit removing actions. Journal of Agricultural Engineering Research 38 (2), 77–90.

Kimmel, E., Peleg, K., Hinga, S., 1992. Vibration modes of spheroidal fruits. Journal of agricultural engineering research 52, 201–213.

Silva, F.M., de Carvalho Alves da, M., de Lima Bueno, R., da Costa, P.A.N. et al., 2012. Geostatistical analysis of fruit yield and detachment force in coffee. Precis. Agric., vol. 13, 1, pp. 76–89.

Savary, S.U., Ehsani, R., Salyani, M., Hebel, M., Bora, G., 2011. Study of force distribution in the citrus tree canopy during harvest using a continuous canopy shaker. Comput. Electron. Agric. 76 (1), 51–58.

Tinoco, H.A., Ocampo, D.A., Peña, F.M., Sanz-Uribe, J.R., 2014. Finite element modal analysis of the fruit-peduncle of Coffea arabica L. var. Colombia estimating its geometrical and mechanical properties. Comput. Electron. Agric. 108, 17–27.

Tinoco, H., Peña, F., 2018. Finite Element Analysis of Coffea arabica L. var. Colombia Fruits for Selective Detachment Using Forced Vibrations. Vibration 1 (1), 207–219.

Adrian, P., Fridley, R., et al., 1958. Mechanical fruit tree shaking: Effect of frequency and stroke on fruit removal and power requirements analyzed in study of reciprocating type shaker. California Agriculture 12 (10), 3–15.

Brewer, H., 1965. Theoretical foundations for an engineering measurement of ease of detachment of individual fruits from a tree at harvest time. Journal of Agricultural Engineering Research 10 (3), 235–240.

Smith, E., Ramsay, A., 1983. Forces during fruit removal by a mechanical raspberry harvester. Journal of Agricultural Engineering Research 28 (1), 21–32.

Gomes, E.Q., Santos, F.L., Nascimento, M., Zanella, M.A., 2020. Transmissibility of coffee fruit-peduncle-branch systems submitted to vibration induced by impact. Dyna 87 (214), 61–65.

Queiroz, D., Santos, F., Pinto, F., 2007. Analysis oh coffee harvesting process by vibration. ASAE Annu. Meet 7, 41–46.

Tavares, T.d.O., de Oliveira, B.R., Silva, V.d.A., Pereira da Silva, R., Dos Santos, A.F., Okida, E.S., times, The, 2019. movements and operational efficiency of mechanized coffee harvesting in sloped areas. PloS one 14 (5), e0217286.

Coelho, A.L.d.F., Santos, F.L., Pinto, F.d.A.d.C., Queiroz, D.M. d., 2015. Detachment efficiency of fruits from coffee plants subjected to mechanical vibrations, Pesquisa Agropecuária Tropical, 45, pp. 406–412.

Zhang, Q., Pierce, F.J., 2013. Agricultural Automation: Fundamentals and Practices. CRC Press.

Norris, C., 2001. Mechanisation of the harvesting of coffee, Coffee Futures. Chinchiná, CABI-FEDERACAFE-USDA-ICO, pp. 44–55.

Butts, T.R., Butts, L.E., Luck, J.D., Fritz, B.K., Hoffmann, W.C., Kruger, G.R., 2019. Droplet size and nozzle tip pressure from a pulse-width modulation sprayer. Biosystems engineering 178, 52–69.

Farooq, M., Balachandar, R., Wulfsohn, D., Wolf, T., 2001. PA–precision agriculture: agricultural sprays in cross-flow and drift. Journal of Agricultural Engineering Research 78 (4), 347–358.

Baio, F.H.R., Pettenan, A.L., Camolese, H., Gabriel, R.R.F., 2016. Evaluation of spray deposits with twin flat tip with air induction in two soybean stages. Idesia 34 (4), 1–6.

Santinato, F., Ruas, R.A.A., Tavares, T.d.O., Silva, R.P.d., Godoy, M.A., 2013. Influence of spray volumes, nozzle types and adjuvants on the control of phoma coffee rust, Coffee Science.

Ivic, S., Andrejcuk, A., Družeta, S., 2019. Autonomous control for multi-agent non-uniform spraying, Appl. Soft Comput., vol. 80, pp. 742–760, ISSN 1568–4946.

Salcedo, R., Zhu, H., Zhang, Z., Wei, Z., Chen, L., Ozkan, E., Falchieri, D., 2020. Foliar deposition and coverage on young apple trees with PWM-controlled spray systems. Comput. Electron. Agric. 178.

Faiçal, B.S., Freitas, H., Gomes, P.H., Mano, L.Y., Pessin, G., de Carvalho, A.C., Krishnamachari, B., Ueyama, J., 2017. An adaptive approach for UAV-based pesticide spraying in dynamic environments. Comput. Electron. Agric. 138, 210–223.

Meng, Y., Su, J., Song, J., Chen, W.-H., Lan, Y., 2020. Experimental evaluation of UAV spraying for peach trees of different shapes: Effects of operational parameters on droplet distribution. Comput. Electron. Agric. 170, 105282.

Ahmad, F., Qiu, B., Dong, X., Ma, J., Huang, X., Ahmed, S., Chandio, F.A., 2020. Effect of operational parameters of UAV sprayer on spray deposition pattern in target and off-target zones during outer field weed control application. Comput. Electron. Agric. 172, 105350.

Vondricka, J., Lammers, P.S., 2009. Real-time controlled direct injection system for precision farming. Precision agriculture 10 (5), 421–430.

Blasco, J., Aleixos, N., Roger, J., Rabatel, G., Molto, E., 2002. Automation and emerging technologies: Robotic weed control using machine vision. Biosystems Engineering 83 (2), 149–157.

Ahmad, J., Muhammad, K., Ahmad, I., Ahmad, W., Smith, M.L., Smith, L.N., Jain, D.K., Wang, H., Mehmood, I., 2018. Visual features based boosted classification of weeds for real-time selective herbicide sprayer systems. Computers in Industry 98, 23–33.

Kuttruff, H., 2006. Acoustics: an introduction. CRC Press.

Ballou, G., 2013. Handbook for sound engineers. Taylor & Francis.

Kleiner, M., 2013. Electroacoustics. CRC Press.

Wilby, J.F., 2009. Vibration of structures induced by sound. In: Piersol, A.G., Paez, T.L. (Eds.), Harris' shock and vibration handbook. McGraw-Hill, New York.

Fahy, F.J., Gardonio, P., 2007. Sound and structural vibration: radiation, transmission and response. Elsevier.

Rechtin, E., Maier, M.W., 2010. The art of systems architecting. CRC Press.

Wainer, G.A., Mosterman, P.J., 2018. Discrete-event modeling and simulation: theory and applications. CRC Press.

Coutinho, C.J.P., 2017. Structural Reduced Scale Models Based on Similitude Theory, Ph. D. thesis, Universidade do Porto (Portugal), 2017.

Coutinho, C.P., Baptista, A.J., Rodriges, J.D., 2018. Modular approach to structural similitude. International Journal of Mechanical Sciences 135, 294–312.

Szücs, E., 1980. Similitude and modelling, vol. 2. Elsevier Science Ltd.

Langhaar, H.L., 1951. Dimensional analysis and theory of models, Tech. Rep., John Wiley & Sons, 1951.

Westine, P.S., Dodge, F.T., Baker, W., 2012. Similarity methods in engineering dynamics: theory and practice of scale modeling. Elsevier.

De Rosa, S., Franco, F., Li, X., Polito, T., 2012. A similitude for structural acoustic enclosures. Mechanical Systems and Signal Processing 30, 330–342.

Coutinho, C.P., Baptista, A.J., Rodrigues, J.D., 2016. Reduced scale models based on similitude theory: a review up to 2015. Engineering Structures 119, 81–94.

Shaw, R.P., Bugl, P., 1969. Transmission of plane waves through layered linear viscoelastic media. The Journal of the Acoustical Society of America 46 (3B), 649–654.

Thiele, N., 1971a. Loudspeakers in vented boxes: Part 1. Journal of the Audio Engineering Society 19 (5), 382–392.

Thiele, N., 1971b. Loudspeakers in vented boxes: Part 2. Journal of the Audio Engineering Society 19 (6), 471–483.

Small, R.H., 1971. Efficiency of direct-radiator loudspeaker systems. Journal of the Audio Engineering Society 19 (10), 862–863.

Small, R.H., 1972. Closed-box loudspeaker systems-part 1: Analysis. Journal of the Audio Engineering Society 20 (10), 798–808.

Small, R.H., 1973. Vented-box loudspeaker systems-part 2: large-signal analysis. Journal of the Audio Engineering Society 21 (6), 438–444.

I. IEC, 60268-5: 2007 Sound system equipment-part 5: Loudspeakers, 2007.

Everest, F.A., 2001. Master handbook of acoustics. ASA.

I.O. for Standardization-ISO, Equipment for crop protection-Methods for field measurement of spray drift, 2005.

MPU-9250 Product Specification, InvenSense Inc., rev. 1.1, 2016.

Temperature and humidity module - AM2302 Product Manual, Aosong Electronics Co., 2015.

BMP280 - Digital Pressure Sensor, Bosch Sensortec GmbH, 1.26, 2021.

Raspberry Pi 3 Model B+, Raspberry Pi Foundation, 2018.

Ground Zero Plutonium GZPA 1.6K-HC Owner's Manual, Ground Zero Mobile Entertainment, 2015.

Instruction Manual SD1000.1D, Soundigital Amplifiers, 2015.

GZIW 12 SPL, Ground Zero, rev. 0, 2017.

Ultravox - Shocker Terremoto 1k2, Ultravox Group, 2015a.

Grand Touring Series - GTO1514D, Harman International Industries, Incorporated, 2012.

Ultravox – Pancadão 2k2, Ultravox Group, 2015b.

PAM8403 Filterless 3W Clas-D Stereo Audio Amplifier, Diodes Incorporated, rev. 1–4, 2012.

Shure S58 User Guide, Shure, rev. 3, 2006.

XENYX X1204USB - User Manual, Behringer, v1.0, 2021.

Jørgensen, L.N., Noe, E., Langvad, A.-M., Jensen, J., Ørum, J.E., Rydahl, P., 2007. Decision support systems: barriers and farmers need for support. EPPO Bull. 37 (2), 374–377.

Balsari, P., Marucco, P., Tamagnone, M., 2007. A test bench for the classification of boom sprayers according to drift risk. Crop Protection 26 (10), 1482–1489.

Karjalainen, M., Ikonen, V., Antsalo, P., Maijala, P., Savioja, L., Suutala, A., Pohjolainen, S., 2001. Comparison of numerical simulation models and measured low-frequency behavior of loudspeaker enclosures. Journal of the Audio Engineering Society 49 (12), 1148–1166.

Ahonen, J., 2003. Equalization of the closed box.

Sahu, K.C., Tuhkuri, J., Reddy, J., 2015. Active attenuation of sound transmission through a soft-core sandwich panel into an acoustic enclosure using volume velocity cancellation. Proceedings of the Institution of Mechanical Engineers, Part C: Journal of Mechanical Engineering Science 229 (17), 3096–3112.

Bezzola, A., Devantier, A., McMullin, E., 2019. Loudspeaker Port Design for Optimal Performance and Listening Experience. In: Audio Engineering Society Convention 147, Audio Engineering Society, 2019.

Júnior, L.d.G.F., da Silva, F.M., Ferreira, D.D., de Souza, C.E.P., Pinto, A.W.M., de Melo Borges, F.E., 2020. Dynamic behavior of coffee tree branches during mechanical harvest, Comput. Electron. Agric. 173, 105415.

Silva, F.C.d., Silva, F.M.d., Alves, M.d.C., Ferraz, G.A., Sales, R.S., et al., 2015. Efficiency of coffee mechanical and selective harvesting in different vibration during harvest time.

Kazama, E.H., da Silva, R.P., Tavares, T.d.O., Correa, L.N., de Lima Estevam, F.N., Nicolau, F.E.d.A., Maldonado Júnior, W., 2021. Methodology for selective coffee harvesting in management zones of yield and maturation, Precis. Agric. 22 (3), pp. 711–733.